

Warm ocean processes and carbon cycling in the Eocene

Journal:	<i>Philosophical Transactions A</i>
Manuscript ID:	RSTA-2013-0099
Article Type:	Research
Date Submitted by the Author:	31-Jan-2013
Complete List of Authors:	John, Eleanor; Cardiff University, Earth and Ocean Sciences Pearson, Paul; Cardiff University, School of Ocean & Earth Sciences Coxall, Helen; Stockholm University, Department of Geological Sciences Birch, Heather; Cardiff University, School of Ocean & Earth Sciences Wade, Bridget; University of Leeds, School of Earth & Environment Foster, Gavin; University of Southampton, Ocean & Earth Science
Issue Code: Click here to find the code for your issue.:	DM1011
Subject:	Biogeochemistry < EARTH SCIENCES, Climatology < EARTH SCIENCES, Geochemistry < EARTH SCIENCES, Geology < EARTH SCIENCES, Palaeontology < EARTH SCIENCES
Keywords:	Eocene, Planktonic foraminifera, Biological pump, Stable isotopes, Carbon cycling, Temperature

SCHOLARONE™
Manuscripts

Warm ocean processes and carbon cycling in the Eocene

BY ELEANOR H. JOHN^{1*}, PAUL N. PEARSON¹, HELEN K. COXALL², HEATHER BIRCH¹, BRIDGET S. WADE³, AND GAVIN L. FOSTER⁴

¹School of Earth & Ocean Sciences, Cardiff University, Cardiff CF10 3AT, UK

*Corresponding author's email: johnEH@cf.ac.uk.

²Department of Geological Sciences, Stockholm University, Svante Arrhenius väg 8, SE-106 91 Stockholm, Sweden

³School of Earth & Environment, University of Leeds, Woodhouse Lane, Leeds, LS2 9JT, UK

⁴Ocean & Earth Science, National Oceanography Centre Southampton, University of Southampton, European Way, SO14 3ZH, UK

Abstract

Sea surface and subsurface temperatures over large parts of the ocean during the Eocene epoch (55.5–33.7 Ma) exceeded modern values by several degrees which must have affected a number of oceanic processes. Here we focus on the effect of elevated water column temperatures on the efficiency of the biological pump, particularly in relation to carbon and nutrient cycling. We use stable isotope values from exceptionally well-preserved planktonic foraminiferal calcite from Tanzania and Mexico to reconstruct vertical carbon isotopes gradients in the upper water column, exploiting the fact that individual species lived and calcified at different depths. The oxygen isotope ratios of different species' tests are used to estimate the temperature of calcification, which we converted to absolute depths using Eocene temperature profiles generated by General Circulation Models. This approach, along with potential pitfalls, is illustrated using data from modern core-top assemblages from the same area. Our results indicate that during the early and middle Eocene, isotope gradients were steeper (and larger) through the upper thermocline than in the modern ocean. This could have been caused by a number of oceanic phenomena but is also consistent with a shallower average depth of organic matter remineralisation. This supports previously proposed hypotheses that invoke high metabolic rates in a warm Eocene ocean, leading to more efficient recycling of organic matter and reduced burial rates of organic carbon.

Index words: Eocene; planktonic foraminifera; biological pump; stable isotopes; carbon cycling temperature.

1. Introduction

1
2
3
4
5
6
7
8
9
10
11
12
13
14
15
16
17
18
19
20
21
22
23
24
25
26
27
28
29
30
31
32
33
34
35
36
37
38
39
40
41
42
43
44
45
46
47
48
49
50
51
52
53
54
55
56
57
58
59
60

There are many concerns about the impact of anthropogenic global warming on the oceans, including changes to thermal structure, circulation patterns, oxygenation and pH (e.g., [1, 2]). The effect of a warmer ocean on the efficiency of the marine biological pump has also been emphasised, due to the fact that respiration rates in remineralising microbes are temperature-dependent (e.g., [3-6]) and may be important for understanding the response of the carbon cycle to current warming trends on short and geological timescales. To predict the effects of warming, these processes can be modelled (e.g., [4]); another approach is to examine them for warm climate states in the past.

During the Eocene epoch (55.5-33.7 Mya), global mean temperatures were undoubtedly higher than today and the poles are thought to have been largely ice-free. Evidence for Eocene warmth in marine and terrestrial realms is diverse and includes records of the distribution of biological taxa (e.g., the presence of cold-blooded animals and frost-intolerant plant species at high latitudes; [7-9]) and analysis of leaf morphology (e.g., [10]). The oxygen stable isotope ratio ($\delta^{18}\text{O}$) of deep sea benthic foraminifera [11-14] shows that bottom waters likely exceeded 10-12 °C in the early Eocene, cooling to 5 °C by the end of the epoch (e.g., [13, 14]). This trend was interrupted by intervals of relatively stability or transient warming events, such as at the Middle Eocene Climatic Optimum (MECO; [15, 16]). Sea surface temperatures, reconstructed using the $\delta^{18}\text{O}$ values of well-preserved planktonic foraminifera [17] and organic proxies also indicate warmer temperatures than the modern throughout the Eocene, particularly at high latitudes (e.g., [18, 19]). Tropical temperatures remained relatively warm and roughly constant during the Eocene, which suggests that the cooling occurred mainly at high latitudes [17, 18]. Although there is some quantitative disagreement between proxies, the general implication that large areas of the open ocean were warmer than the modern for most of the Eocene is sound, and it is unlikely that global Eocene temperatures have been exceeded since.

Elevated seawater temperatures could have affected the state of the Earth system in many ways, for example causing changes in ocean circulation, evaporation patterns, cloud formation, latent heat transfer to the atmosphere and increased storminess over large areas [20, 21]. Higher ocean temperatures may also have affected the biological pump, that is, the biologically-mediated transport of organic carbon out of the surface ocean to the ocean interior before it is remineralised back to CO_2 (e.g. [22]; Fig. 1). Bacterial respiration is one of the main ways that sinking organic matter is decomposed and carbon and nutrients that were fixed near the surface through photosynthesis are recycled at depth. Because the metabolic rates of these remineralising bacteria are temperature-dependent, elevated ocean temperatures may result in more efficient recycling of carbon and nutrients higher in the water column thus affecting the amount of sinking carbon that

1 reaches the deep sea and sea floor sediments. Because microbial respiration produces CO₂ this
2 would also alter the distribution of dissolved inorganic carbon (DIC) in the water column as well as
3 potentially affecting atmospheric CO₂. If the oceans were indeed globally warmer during the
4 Eocene, these effects may also have been global and therefore need to be addressed if we are to
5 understand global carbon cycling. This was emphasised by Olivarez Lyle and Lyle [23] who
6 postulated that higher Eocene temperatures and enhanced remineralisation rates were responsible
7 for reduced organic carbon burial rates in the deep sea. Such effects may have been an important
8 feedback on global climate throughout the Phanerozoic [4, 24].
9

10 Bacterial remineralisation of organic matter also results in the redistribution of carbon isotopes in
11 the water column: photosynthetic carbon fixation in the photic zone preferentially removes ¹²C
12 leaving the remaining DIC pool with elevated δ¹³C_{DIC} values; upon sinking, microbes respire this
13 organic matter and return the isotopically light carbon to the DIC pool. This is reflected in a general
14 decrease in δ¹³C_{DIC} values with depth in the upper part of the water column (Fig. 1). Potentially,
15 depth stratified planktonic foraminifera can also record this process of organic matter
16 remineralisation as a decrease in the δ¹³C of their test calcite with increased water depth habitat
17 (e.g., [25]). The actual shape of δ¹³C_{DIC}:depth profiles are highly variable worldwide and among the
18 main controls on the shape of the profile are the depth and efficiency of remineralisation processes
19 in the water column.
20
21
22
23
24
25
26
27
28
29
30
31
32
33
34

35 In this contribution we investigate these effects by using assemblages of exceptionally well-
36 preserved planktonic foraminifera from the Eocene of Tanzania and Mexico to reconstruct the
37 vertical gradient of stable carbon isotope ratios in DIC (δ¹³C_{DIC}) in the water column for various
38 timeslices throughout the epoch. This has not previously been carried out using foraminifera that
39 have not been subject to the micron-scale recrystallization that is common in deep sea carbonates;
40 this is important because such recrystallization can dampen surface-to-deep δ¹³C_{DIC} offsets. We use
41 these profiles to decipher information about water column processes, including the efficiency of the
42 biological pump during the Eocene in comparison with today.
43
44
45
46
47
48
49

50 **2. The Metabolic Hypothesis and the Q₁₀ relationship**

51
52
53 There is a rich literature on the effects of temperature on biological activity. Arrhenius [26]
54 described the exponential increase in inorganic reaction rates with temperature in terms of 'Q₁₀', the
55 fractional increase in reaction rate for every 10 °C increase in temperature. It has long been known
56 that metabolic rates in ectothermic organisms also follow the Q₁₀ pattern and show a very
57
58
59
60

1 approximate doubling per 10 °C increase (i.e. $Q_{10} = \sim 2.0$). This includes marine and terrestrial
2 microbial decomposers whose measured Q_{10} activities lie between ~ 2 and 4 [27-31]. The Q_{10}
3 pattern can also be used to describe the temperature dependence of metabolic rates in a more
4 diverse range of life forms, from unicellular ectotherms to large endothermic mammals, with other
5 factors such as body size playing important additional roles; these relationships have been expanded
6 to describe entire complex ecosystems in terms of the role that temperature plays in regulating an
7 ecosystem's 'metabolism' [32-34].
8
9

10 Theory predicts that metabolic rates in all oceanic planktonic communities should be strongly
11 dependent on temperature (e.g., [32-36]). Importantly, while both rates of respiration and rates of
12 photosynthesis should increase with increasing temperature, the effect of temperature is stronger on
13 heterotrophic communities (respirers) than it is on autotrophic communities (photosynthesisers)
14 [36] leading to an increasing dominance of heterotrophic activity in warmer waters. This has been
15 demonstrated in the modern oceans [3, 6, 37]. Based on a large database of 1156 volumetric
16 estimates of oceanic planktonic metabolism and temperature measurements, Regaudie-de-Gioux
17 and Duarte [6] demonstrated strong relationships between both gross primary production and
18 community respiration rates and temperature and found average Q_{10} values for the whole ocean of
19 1.56 for gross primary production and 2.52 for community respiration. The rates of increase in
20 metabolism with temperature were comparable in the two hemispheres but different between ocean
21 basins and between seasons, reflecting changes in planktonic community structure. The positive
22 relationship between temperature and the ratio of heterotrophic/autotrophic activity appears to be
23 strong below 20-21 °C [3, 6] with a weaker relationship at higher temperatures due to an overall
24 dominance of heterotrophs [3]. Feedbacks on the global carbon cycle are likely because areas of net
25 heterotrophy represent sources of CO_2 to the atmosphere provided there is an allochthonous source
26 of food for the microbes [37].
27
28
29
30
31
32
33
34
35
36
37
38
39
40
41
42
43
44

45 These relationships also have a bearing on the biological pump as enhanced rates of organic carbon
46 remineralisation could reduce the amount of carbon reaching the deep ocean and the seafloor. Laws
47 et al. [3] used a complex pelagic food web model to investigate controls on modern export
48 production including ecological interactions, controls on the metabolic rates of different organisms
49 and other dynamic processes. They concluded that temperature variations could account for >80 %
50 of the variance in their modelled export production. Several studies have used modelling results to
51 emphasise the affect of temperature-dependent remineralisation on the strength of the organic
52 carbon pump, atmospheric CO_2 and nutrient distribution in the ocean, primarily on glacial-
53 interglacial timescales where we have a wealth of data to cross-check with the model. Matsumoto
54
55
56
57
58
59
60

1 [4] used results from an intermediate-complexity climate model to account for around a third of the
2 changes in CO₂ between Plio-Pleistocene glacials and interglacials by invoking suppressed
3 microbial activity and a stronger organic pump strength during colder glacials. This led to a lower
4 relative export rate of CaCO₃ versus C_{org} to the deep seafloor (i.e., a lower 'rain ratio'). From a
5 comprehensive map of rain ratios and their high resolution regional ocean ecosystem model
6 Matsumoto [4] proposed that today's rain ratios are controlled at least in part by temperature
7 through both enhanced remineralisation of organic matter and temperature dependence of
8 community composition. Chikamoto et al. [38]'s model simulations include temperature-dependent
9 remineralisation rates and these authors came to similar conclusions about the importance of
10 temperature in controlling export production.
11
12
13
14
15
16
17
18
19

20 Although some authors have warned that global increases in ocean temperature could result in both
21 increased *p*CO₂ levels and decreased rates of burial of organic carbon (e.g. [4]), these ideas have
22 been little discussed in relation to the warm oceans of the Eocene or indeed other warm climates of
23 the past. However, it seems clear that the effects of temperature on the biological pump could have
24 strong implications for our understanding of controls on carbon cycling in ancient greenhouse
25 worlds. Gu et al. [39] proposed that a warmer ocean would increase rates of methanogenesis in
26 seafloor sediments thus providing a source for the isotopically light carbon released during Eocene
27 hyperthermals. However, a warmer ocean would presumably also affect rates of aerobic respiration
28 of sinking organic matter in this context. Olivarez Lyle and Lyle [23] suggested that the
29 discrepancy between percentages of biogenic Ba (an indicator of primary productivity) and organic
30 matter preserved in early Eocene sediments from the equatorial Pacific could be explained through
31 increases in microbial respiration rates in a warmer ocean and a subsequent reduction in the burial
32 rate of organic carbon. They also suggest that increased dissolved inorganic carbon (DIC)
33 concentrations in the water column (caused by enhanced biogenic production of CO₂) relative to
34 alkalinity inputs from weathering on land and subsequent shoaling of the carbonate compensation
35 depth (CCD) would lead to reduced inorganic carbon burial. This relatively simple model involving
36 positive feedbacks was suggested as a mechanism for maintaining high *p*CO₂ levels in greenhouse
37 worlds and inversely low greenhouse gas concentrations in icehouse worlds ([23], see also [24]).
38
39
40
41
42
43
44
45
46
47
48
49
50

51 There are various complications with these ideas. For example, it is difficult to conceive how
52 elevated *p*CO₂ levels can be maintained by these processes in light of the tight inorganic feedbacks
53 that mediate atmospheric CO₂ change, such as silicate weathering [40]. It has also been suggested
54 that calcium carbonate, the dominant test mineralogy among Eocene plankton, is a more effective
55 ballasting agent than biogenic opal, which dominates planktonic communities today, more rapidly
56
57
58
59
60

1 transporting organic matter to the seafloor for subsequent burial [41-43] although recent work
2 suggests that the importance of mineral ballasting may have been over-estimated [44]. The effects
3 of enhanced remineralisation on oxygen concentrations should also be carefully considered as
4 oxygen (produced during photosynthesis) is consumed during microbial respiration. The effects on
5 the distribution of oxygen minimum zones (OMZ) in the oceans should also be considered although
6 at present the distribution of OMZs is mainly controlled by large-scale circulation patterns. Despite
7 these considerations, it is clear that there were likely radical differences between the ways in which
8 the marine biological pump operated in the warm Eocene compared with today; this study represent
9 an attempt to detect such differences using the stable isotope record of foraminiferal calcite.

10 11 12 13 14 15 16 17 18 19 **3. The Tanzania foraminifer stable isotope record**

20 Foraminifera are unicellular protists that are abundant in oceanic environments. Some species are
21 benthic; others live as plankton, with habitats distributed through the upper part of the water column
22 (e.g.,[45]). Foraminifera secrete 'tests' (shells) of calcium carbonate that accumulate on the sea
23 floor after death and can be a major component of pelagic sediments. A suite of geochemical
24 proxies can be extracted from foraminifer tests to provide information about the water in which they
25 calcified; here we focus on a combination of oxygen and carbon isotope ratios.

26 The oxygen isotope ratio of calcite is dependent in part on the temperature of the water in which it
27 calcified: $\delta^{18}\text{O}$ values increase with water depth in accordance with the accompanying decrease in
28 temperature (e.g., [12, 46]). The carbon isotope ratio of calcite depends largely on that of the
29 bicarbonate ion, HCO_3^- , from which it precipitated [47] which, in turn, reflects air-sea exchange
30 processes in the surface ocean and biological activity. There is a non-linear relationship between
31 $\delta^{13}\text{C}_{\text{DIC}}$ and depth because of the photosynthetic fixation of isotopically light carbon in the surface
32 ocean and its subsequent remineralisation at depth (Fig. 1). However, stable isotope ratios in
33 foraminiferal tests are also affected by other factors, which mean that calcification does not occur in
34 isotopic equilibrium with ambient seawater (see below). Insights into such disequilibrium effects in
35 modern assemblages were made by Birch et al. ([48]; Section 4) and their observations are applied
36 in this study.

37 Here we use stable isotope ratios of planktonic foraminifera from Eocene hemipelagic sediments of
38 Tanzania as published as Supplementary Information to Pearson et al. [17] and in Wade and
39 Pearson [49] and from an Eocene shale of eastern Mexico (the Guayabal Formation), as published
40 in Pearson et al. [50]. The significance of the carbon isotope data has not previously been discussed.

1
2 These Tanzanian and Mexican data are particularly valuable as they are derived from exceptionally
3 well-preserved assemblages with no evidence of micron-scale recrystallization ([17, 50]; see also
4 [51]). This is important because such diagenesis can have a large effect on the stable isotope
5 composition of foraminiferal tests, including $\delta^{13}\text{C}$ [17, 52], despite claims to the contrary (e.g.,
6 [53]). The Tanzanian assemblages represent those typical of open ocean conditions, complete with
7 deep dwelling forms, and were deposited in an upper bathyal environment [54, 55]. The single
8 Mexican dataset also represents a typical open ocean assemblage. The ages of the core samples are
9 determined by foraminiferal and nannofossil biostratigraphy [17, 50]. Recent advances in Eocene
10 biostratigraphy have resulted in significant changes in the ages of several bioevents in the earliest
11 middle Eocene; we have therefore updated the age of each sample in comparison to the previous
12 publications as per Wade et al. [56]. The Tanzanian samples range in age between 54.90–33.75 Ma
13 and the single Mexican sample is dated at 42.05 ± 1.55 Ma. During these times relatively warm
14 conditions prevailed in Tanzania and eastern Mexico with reconstructed sea surface temperatures in
15 the range 30–34.5 °C [17, 49, 50] (compared with 29–30 °C for the modern; [48]).
16
17
18
19
20
21
22
23
24
25
26

27 **4. Multi-species and dissolved inorganic carbon in the modern**

28
29
30 In this section we describe the approach of reconstructing water column $\delta^{13}\text{C}_{\text{DIC}}$ gradients using
31 stable isotope data from foraminiferal assemblages by summarising data from a modern core-top
32 assemblage from offshore Tanzania, as studied by Birch et al. [48]. Although limited to one
33 location, this study is useful in presenting data from a wide range of planktonic foraminifera shell
34 sizes (80–800 μm , taxon dependent) for each species investigated. The results provide new insights
35 into foraminiferal test $\delta^{13}\text{C}$ variability that refine our ability to recognise several vital effects,
36 including disequilibrium effects, in geochemical data from fossil assemblages.
37
38
39
40
41
42

43 Birch et al. [48] measured $\delta^{13}\text{C}$ and $\delta^{18}\text{O}$ values in 12 species of planktonic foraminifera from a
44 single core-top sample. Using a series of sieves with increasing mesh size, a total of 60 species-
45 specific, size-controlled splits were separated (each consisting of multiple shells) so that the effects
46 of size and species on the isotope ratios could be investigated in detail. Figure 2 shows the $\delta^{13}\text{C}$ and
47 $\delta^{18}\text{O}$ data from the multispecies size fraction splits plotted against each other. The variability along
48 the $\delta^{18}\text{O}$ axis primarily reflects the depth of calcification (with warmer waters, i.e. lower $\delta^{18}\text{O}$
49 values, near the surface) and seasonal variations. Birch et al. first used their $\delta^{18}\text{O}$ values to
50 determine temperature using the equation of Erez and Luz [57] and then overlaid this temperature
51 on the measured water column temperature profile to estimate absolute depth of calcification. They
52 used water column $\delta^{13}\text{C}_{\text{DIC}}$ measurements from a range of locations near their study site to
53
54
55
56
57
58
59
60

1
2 determine the approximate values that would result if the foraminifer tests had calcified in
3 approximate isotopic equilibrium with ambient seawater temperature and $\delta^{13}\text{C}_{\text{DIC}}$ under conditions
4 of 'normal' water column structure. Measurements from a range of settings (~2500 m to >5000 m
5 water depth) within ~800 km of their study site [82] yielded similar shaped profiles and absolute
6 values and a compilation of these values is represented by a grey band in Figure 1 (see [48] for
7 details). The width of the band was also intended to account for seasonal effects. The fact that Birch
8 et al.'s data do not all fall close to this band or any single line in Figure 2 implies that other factors
9 are influencing the $\delta^{13}\text{C}$ values. The position of the data with respect to the typical 'equilibrium
10 line' helps demonstrate four main types of effect (illustrated in Figure 2):
11
12
13
14
15
16
17

- 18 1) *The metabolic fractionation effect.* Foraminifera that are smaller than the 212 μm sieve size
19 (either adults of relatively small species or the juvenile stages of larger species) tend to have
20 $\delta^{13}\text{C}$ values that are more negative than ambient seawater, the offset being greatest for the
21 smallest size fractions [58]. This is thought to be due to the incorporation of a fraction of
22 isotopically light carbon from organic matter that has previously been respired by the
23 foraminifer itself. The fraction of metabolic carbon in the foraminifer test decreases as the
24 foraminifer grows, as the rate of metabolic activity decreases and exchange of carbon with
25 ambient seawater improves [58-63].
26
27
- 28 2) *The photosynthetic fractionation effect.* Many species of near-surface dwelling planktonic
29 foraminifera have a symbiotic relationship with photosynthesizing algae, mainly
30 dinoflagellates. These algae preferentially remove ^{12}C during photosynthesis, leaving the
31 remaining seawater isotopically heavy with respect to ambient DIC; such locally elevated
32 $\delta^{13}\text{C}$ values may then be recorded by the foraminifera [25, 64-69]. As foraminifera grow to
33 larger sizes, so the cloud of algae surrounding the foraminifer test increases and the
34 photosynthetic effect is increasingly pronounced in successive size fractions. This becomes
35 particularly marked in the tests of symbiotic species over about 355 μm in diameter [48].
36
37
- 38 3) *The pH fractionation effect.* A few species are adapted to deep-water habitats close to the
39 oxygen minimum zone where the pH is reduced. Such species may have $\delta^{13}\text{C}$ values that
40 show a positive offset from equilibrium values and it has been postulated that this is due to
41 pH-dependent fractionation effects [47, 48, 70].
42
43
- 44 4) *The seasonal upwelling effect.* Certain species, including *Globigerina bulloides* and the
45 small species *Globigerinita glutinata*, as discussed in the study of Birch et al. [48], together
46 with *Neogloboquadrina dutertrei* [71-73] are indicative of more productive tropical surface
47 conditions linked to seasonal upwelling [72-74]. The $\delta^{13}\text{C}$ composition of such species' tests
48 is therefore more similar to that of deeper-dwelling species because they record the isotopic
49
50
51
52
53
54
55
56
57
58
59
60

1 chemistry of cool, ^{12}C -rich, upwelling deep waters. It should be noted however that these
2 species only make up a small proportion of those presented in Figure 1 which otherwise
3 resembles an oligotrophic assemblage [48].
4
5
6
7

8 To counteract these effects when reconstructing the water column $\delta^{13}\text{C}_{\text{DIC}}$ gradient, Birch et al. [48]
9 recommend that surface mixed layer $\delta^{13}\text{C}$ values are best estimated using foraminifera in the middle
10 of their size range, i.e. 212-355 μm (Fig. 2), and if deep-dwelling species show unexpected scatter
11 in their $\delta^{13}\text{C}$ values, then ambient $\delta^{13}\text{C}$ is best estimated using the more negative values. From
12 Figure 2 it can be seen that these relatively simple rules apply reasonably well to the modern data
13 set. Some scatter is always expected due to seasonal and inter-annual variability in water column
14 structure and chemistry at any given site. Another complication is that some species might change
15 their position in the water column during its life cycle; in particular, some surface dwelling
16 symbiotic forms sink in their final life stages to reproduce, forming a crust of gametogenic calcite
17 [64]. The measured stable isotope values in adult size fractions of such species will plot on a mixing
18 line between the two depth habitats (Figs. 2, 3). This effect is not obvious in the modern data of
19 Birch et al. [48] although it may be responsible for some of the differences in $\delta^{18}\text{O}$ between
20 symbiont-bearing species such as *Globiginerinoides sacculifer*, *G. ruber* and *Orbulina universa*. It
21 does, however, seem to be more pronounced in data from certain genera of fossil planktonic
22 foraminifera (see below). Figure 3 is a simple interpretative cartoon modified from Pearson and
23 Wade [75] summarizing these effects and how they can be identified in the fossil data sets used in
24 this study.
25
26
27
28
29
30
31
32
33
34
35
36
37
38

39 5. Eocene reconstructions

40
41 We reconstructed water column $\delta^{13}\text{C}_{\text{DIC}}$ profiles for several Eocene timeslices by the following four
42 steps:
43
44

- 45 1) We plotted the $\delta^{18}\text{O}$ and $\delta^{13}\text{C}$ values for each species/size fraction against each other and
46 used the criteria of Birch et al. [48, 76] discussed above to identify those data points that are
47 considered to represent disequilibrium/upwelling effects or that plot along a mixing line
48 between two distinct depth habitats (Fig. 3). We used an optimal growth stage/shell size
49 window of 212-355 μm .
50
51
- 52 2) The $\delta^{18}\text{O}$ values for the chosen species/size fractions were converted into calcification
53 temperatures using the equation of Kim and O'Neil [77]. We used an Eocene ice volume
54 correction of -0.75 ‰ according to Cramer et al. [78] and we applied a seawater latitude
55 correction of +0.83 [79] assuming a palaeolatitude of 19°S.
56
57
58
59
60

- 3) The depth of calcification for each of these samples was estimated by fitting these $\delta^{18}\text{O}$ temperatures to modelled Eocene water column temperature profiles for offshore Tanzania and the south-east Gulf of Mexico [80, 81].
- 4) We plotted the corresponding $\delta^{13}\text{C}$ values against the reconstructed calcification depth for each data point. The resulting Tanzanian $\delta^{13}\text{C}_{\text{DIC}}$:depth profiles were compared to the modern profile for offshore Tanzania (a composite of the profiles used in Birch et al. [48], from the World Ocean Database 2009 [82], is shown in Fig. 5 A-Giv).

To carry out step 3), Eocene temperature:depth profiles for offshore Tanzania and the south-east part of the Gulf of Mexico were extracted from published Eocene General Circulation Model reconstructions. In the case of Tanzania these were generated by the NCAR (National Center for Atmospheric Research) model and also the HadCM3 (Hadley Centre Model, version 3) model for comparison. The NCAR model profile [81] was generated for a continental margin adjacent to the east African coast centred around a latitude of $\sim 18.2^\circ\text{S}$ and for a slope extending from 0 m water depth down to a water depth of 1500 m (Fig. 4). Experiments using different climate forcings of 1120, 2240 and 4480 ppmv atmospheric $p\text{CO}_2$ changed the absolute temperatures but not the shape of the temperature:depth profiles. We selected the profile generated by the $p\text{CO}_2$ condition that produced sea surface temperatures consistent with those estimated from the mixed layer foraminiferal $\delta^{18}\text{O}$ data from our multispecies dataset [17]. For example, the profile generated using 4480 ppmv $p\text{CO}_2$ was used for the early Eocene assemblages, and those generated using 2240 ppmv and 1120 ppmv $p\text{CO}_2$ were used for the middle Eocene and late Eocene timeslices, respectively. In the different $p\text{CO}_2$ scenarios, the temperature gradient between the surface and 1500 m was always 18-20°C and, at all depths, even near the coast and at maximum water depths, most of the temperature gradient is above 600 m; i.e. this reconstruction should be relevant even for the shallower palaeodepth estimates. For the HadCM3 model [80], a forcing of 1680 ppmv $p\text{CO}_2$ was applied and the generated profile (Fig. 4) represents that for a grid box centred around 41.25°E and 20°S for a water depth of up to ~ 4500 m. The shapes of the profiles generated by the two different models are consistent and both show distinct differences compared with the modern profile for offshore Tanzania (from in situ temperature measurements; Fig. 4). Not only are the Eocene temperature:depth profiles offset to warmer temperatures over the entire water column compared with the modern Tanzania profile, the overall surface-to-deep temperature offsets are smaller. The thermocline is also broader in the Eocene profiles with a roughly constant rate of temperature change down to 600 m compared with a modern thermocline that extends down to ~ 150 m. To determine the absolute depths for our foraminifera sample data, we used a logarithmic regression of the data generated by the NCAR model from the surface to a depth of 600 m (as this was most

1 consistent with the hemipelagic slope setting and benthic $\delta^{18}\text{O}$ temperature estimates). The $\delta^{18}\text{O}$ -
2 derived temperatures for each data point (derived in Step 2) were input into the equation generated
3 by this regression to give an absolute water depth. For the single dataset from the Guayabal
4 Formation, Mexico, a temperature:depth profile was also generated using the NCAR model [81]
5 and a climate forcing of 2240 ppmv $p\text{CO}_2$ for an area in the south-east part of the Gulf of Mexico
6 from the coast down to 1500 m water depth (Fig. 4). Modern temperature:depth measurements for
7 this area were obtained from the World Ocean Atlas 2009 database [83]; the curve in Figure 4
8 represents a composite of 7 profiles between 19.5 and 22.5 N and -95.5 and -96.5 W. Both profiles
9 are also shown in Figure 4. A logarithmic regression of the data generated by the NCAR model
10 from the surface to a depth of ~300 m (consistent with the neritic zone palaeoenvironment of the
11 Guayabal Formation) and absolute water depths determined as for Tanzania. The significance of the
12 model results are discussed in Tindall et al. [80] and Huber et al. [81].

23 The carbon and oxygen isotope crossplots and the step-by-step reconstruction of the $\delta^{13}\text{C}_{\text{DIC}}$:depth
24 profiles are illustrated in Figure 5. The mixed layer species, that is those with the lowest $\delta^{18}\text{O}$
25 values, in the early and middle Eocene samples are mainly from the muricate genera *Acarinina*,
26 *Morozovella*, *Morozovelloides* and *Igorina* which are interpreted as having had obligate symbiotic
27 algae [67, 84, 85]. The majority of symbiotic $\delta^{13}\text{C}$ enrichment in these species, which has the effect
28 of exaggerating the surface-to-deep $\delta^{13}\text{C}_{\text{DIC}}$ gradient, has been minimised by only using species
29 within the 212-355 μm test size range, as discussed above (Fig. 5Aii-Fii). Other near-surface
30 calcifiers include the apparently non-symbiotic genera *Pseudohastigerina*, *Planoglobanomalina*
31 [86] and *Chiloguembelina* [87]. Other genera present include *Dentoglobigerina*, *Turborotalia*,
32 *Parasubbotina*, *Subbotina*, *Hantkenina* and *Catapsydrax* whose lower $\delta^{13}\text{C}$ and higher $\delta^{18}\text{O}$ values
33 indicate calcification at greater depths. Species belonging to the genera *Globigerinatheka*,
34 *Orbulinooides*, and *Guembelitrioides* tend to have isotopic compositions suggestive of mixed layer
35 calcification followed by further gametogenic calcification at greater depth. This is consistent with
36 observations as these genera typically show gametogenic calcite crusts (e.g., [84, 88]; hence these
37 data were not used to generate the $\delta^{13}\text{C}$:depth profiles (Fig. 5).

50 The one late Eocene assemblage (Fig. 5G) differs in composition from the others in part due to the
51 large assemblage turnover in planktonic foraminifera in the late middle Eocene that resulted in the
52 extinction of the morozovelloidids and larger acarininids [89]. Constructing a realistic $\delta^{13}\text{C}$ profile
53 for this assemblage is problematic given the limited mixed layer data. We include the plots for
54 completeness but restrict our interpretation to the early and middle Eocene reconstructions pending
55 further investigation of late Eocene assemblages.

1
2
3
4 There are two common features to the early and middle Eocene profiles:

- 5
6
7
8
9
10
11
12
13
14
15
16
17
18
19
20
21
22
23
24
25
26
27
28
29
30
31
32
33
34
35
36
- 1) The carbon isotope profile appears to have been much steeper through the upper thermocline than is typical of the oceans in this area and most of the world. The modern $\delta^{13}\text{C}$ profile for this part of the Indian Ocean [48, 82] shows a fairly constant rate of decrease down to ~1 km, with little change beyond this depth. Conversely, the early and middle Eocene profiles consistently show a sharp decrease in $\delta^{13}\text{C}$ concentrated between the mixed layer and ~100-150 m depth.
 - 2) The overall surface-to-deep offsets in the early and middle Eocene $\delta^{13}\text{C}$ profiles are large relative to today, even when the Suess effect is taken into account. In the modern western Indian Ocean at this latitude the total gradient is ~1-1.5 ‰. On a global scale, modern surface-to-deep gradients rarely exceed 2 ‰ [90]. Similar gradients have also characterised at least the last 20 million years [91]. However, the early and middle Eocene profiles show $\delta^{13}\text{C}$ offsets of 2-4 ‰. Similar values, and overall surface-to-deep gradients (2-3 ‰), have been previously reported for the early and middle Eocene even from recrystallised foraminifera from a variety of latitudes in the Atlantic, Pacific, Indian and Mediterranean basins (e.g., [50, 53, 92]); recrystallisation should dampen surface-to-deep $\delta^{13}\text{C}$ gradients as measured in foraminifera tests and so many of these datasets may underestimate the offsets. In terms of absolute values, surface values in our dataset are mostly elevated compared with today; deepwater values are comparable.

37
38
39
40
41
42
43
44
45
46
47
48
49
50
51
52
53
54

We consider it unlikely that features 1) and 2) are an artefact of the modelled water column temperature:depth profile. For example, if the modelled profiles had underestimated the temperature gradient in the upper ocean and the profile shape was more similar to the modern, the reconstructed $\delta^{13}\text{DIC}$:depth gradients would be even steeper through the upper thermocline as the range of $\delta^{18}\text{O}$ values (and therefore temperature) measured in the assemblage is small. However, if the models had *overestimated* the temperature:depth gradient and water column temperatures were actually more vertically homogenous, we could admittedly have generated a $\delta^{13}\text{DIC}$:depth gradient that was artificially steep in the upper ocean. Nonetheless, the large range of $\delta^{13}\text{DIC}$ values measured in the Tanzanian and Mexican foraminifera assemblages suggests that strong vertical mixing was not occurring at those sites.

55
56
57
58
59
60

Another potential source of uncertainty relates to the issue of Eocene water depths and coastal proximity which can be difficult to determine precisely for hemipelagic deposits and may have varied with time. The Kilwa Group of Tanzania comprises several kilometre successions of

1 relatively monotonous clays and claystones with occasional turbidite interbeds [54, 55]. The
2 palaeoshoreline is estimated to have been generally about 50 km from the site of deposition [93]
3 and palaeodepths have previously been estimated at 300-500 m based on upper bathyal benthic
4 foraminiferal assemblages (e.g., [55]). However, the deeper limit of this estimate is very uncertain,
5 and given the narrow shelf and steep slope that is typical of the East Africa margin, it is quite
6 possible that palaeodepths were considerably greater than this. Both the foraminifera and
7 nannofossil assemblages indicate a fairly constant, open, deep, and relatively oligotrophic
8 environment; there are no restricted assemblages or conspicuous shelf-restricted or eutrophic taxa
9 [51]. Coring of modern hemipelagic sediments offshore Tanzania has revealed that silty clays of
10 similar facies to the Kilwa Group are currently being deposited at depths of 500 m to 1800 m within
11 50 km of the shoreline [94] hence a more conservative depth estimate for the Eocene sediments
12 would be 300 – 1800 m. For both modern and Eocene environments it is likely that onshore
13 currents brought gyre water onto the continental slope, lending an oceanic rather than coastal
14 character to the water column. Therefore, although we acknowledge that these issues do introduce
15 uncertainty into our approach, we also argue that it is not reasonable to rule out the idea that the
16 Eocene and modern datasets represent similar palaeoenvironments.
17
18
19
20
21
22
23
24
25
26
27
28
29

30 In addition, although all Eocene planktonic foraminifera are extinct, we can envisage no plausible
31 vital effect or other fractionation factor that would have affected the surface dwelling forms in a
32 way that could produce such heavy $\delta^{13}\text{C}$ values as seen in Figure 5. Even if we have inadvertently
33 included values affected by symbiotic effects, such effects are only $\sim 1\text{‰}$ or less in the modern and
34 can therefore not explain the differences fully. An obvious question, then, is to ask whether these
35 surface dwellers had more pronounced symbiotic effects than modern forms. It may also be that the
36 isotopic fractionation factor associated with primary production (i.e. that associated with symbionts)
37 was higher before the late Eocene due to effects relating to elevated $p\text{CO}_2$ levels, growth rates
38 and/or volume to surface area ratios in primary producers [95, 96]. However, published
39 relationships between $\delta^{13}\text{C}$ and test size for muricate species (acarininids and morozovellids) from
40 warm Palaeocene/Eocene oceans have similar or indeed shallower gradients to modern planktonic
41 foraminifera with obligate symbionts, such as *Globigerinoides ruber* and *Gs. sacculifer* [67, 76, 97,
42 98] suggesting that, if anything, the symbiotic effect was less pronounced. Hence the data suggest
43 that vertical carbon cycling operated very differently in the early and middle Eocene than is typical
44 in the modern ocean.
45
46
47
48
49
50
51
52
53
54
55

56 **6. Interpretation**

57
58
59
60

1 The fact that the $\delta^{13}\text{C}_{\text{DIC}}$ decreases so sharply through the upper thermocline and to such a degree in
2 the Eocene time slices compared with most modern oceanic environments is notable. One control
3 on the depth of the $\delta^{13}\text{C}_{\text{DIC}}$ minimum is oceanic circulation and different oceanic circulation/mixing
4 patterns in the Eocene compared with the modern, for example a shallower mixed layer (perhaps
5 due to reduced wind induced mixing), or enhanced oceanic stratification relating to a warmer
6 climate, could have contributed to the sharper, shallower decrease in $\delta^{13}\text{C}_{\text{DIC}}$. Additionally, faster
7 rates of remineralisation of sinking organic matter below the mixed layer could partly explain the
8 shape of the profile. Indeed, the shape of the profiles imply that the majority of remineralisation of
9 sinking organic matter was occurring at a much shallower depth than is typical in the modern.

10 Reconstructed sea surface temperatures offshore Tanzania and the Gulf of Mexico in the Eocene
11 were only about $\sim 2\text{-}4\text{ }^{\circ}\text{C}$ greater than today which is not sufficient to affect remineralisation rates
12 greatly, particularly at temperatures so much higher than $\sim 20\text{ }^{\circ}\text{C}$. However, at a depth of $\sim 150\text{ m}$,
13 Eocene water temperatures were $\sim 10\text{ }^{\circ}\text{C}$ higher than today (Fig. 4; [80, 81]); this means that if, for
14 example, heterotrophic community respiration had a Q_{10} value of 2 (a conservative estimate, e.g.
15 [6]), respiration rates could quite reasonably have been twice as high at these depths than in the
16 modern. Therefore, any temperature-related increase in microbial metabolic activity rates would
17 have been more pronounced below the mixed layer than at the surface, that is, in the zone of net
18 respiration rather than net photosynthesis. We acknowledge that there are controls on the shape of
19 the vertical $\delta^{13}\text{C}_{\text{DIC}}$ profile other than temperature-dependent remineralisation and that to
20 understand how these factors affect how $\delta^{13}\text{C}_{\text{DIC}}$ changes with depth requires detailed modelling.
21 However, we propose here that the shape of the $\delta^{13}\text{C}_{\text{DIC}}$:depth profile could have resulted, at least in
22 part, from the fact that there was a much greater temperature difference at depths below the mixed
23 layer (Fig. 4) which in turn led to more rapid rates of organic matter remineralisation.

24 If biogenic remineralisation of organic carbon was more efficient in the Eocene water column due
25 to elevated water temperatures, given that warmer-than-modern water temperatures extended to
26 high latitudes, these findings may have had global significance. As proposed by Olivarez Lyle and
27 Lyle [23], Stanley [24], and other authors focusing on the importance in terms of modern climates
28 (e.g., [3, 4, 6]) this may have affected the transport of organic matter to the deep ocean and may
29 have ultimately reduced rates of organic carbon burial and indeed inorganic burial through an
30 increase in the DIC reservoir a shoaling of the carbonate compensation depth (CCD). This could
31 have pushed $p\text{CO}_2$ levels even higher thus supporting a positive feedback mechanism keeping $p\text{CO}_2$
32 levels high during greenhouse periods (when remineralisation rates are high) and low during
33 icehouse conditions (when remineralisation rates are lower). However, the possibility of global
34 effects are probably best investigated using carbon cycle modeling, because, for example, any

1
2 consideration of impacts on the global carbon cycle must also take into account organic carbon
3 burial and remineralisation rates in continental shelf environments (e.g., [96, 99, 100]). Rapid
4 subsurface bacterial remineralisation would also have caused a marked upward displacement of the
5 oxygen minimum zone which would have in turn have affected the locus and rate of organic carbon
6 deposition on the continental shelves and margins [24]. Moreover on long timescales (e.g. 10^3 - 10^6
7 years) negative feedback mechanisms caused by enhanced silicate weathering could counteract any
8 increases in $p\text{CO}_2$ caused by a reduction in deep sea carbon burial (e.g., [99, 101, 102]).
9

10
11
12
13
14
15 The second observation, that is, the larger surface-to-deep $\delta^{13}\text{C}$ gradient, has been reported in
16 several cases and seems to be a common feature of the Eocene ocean [53, 92]. More complete
17 remineralisation of organic matter should in theory produce a greater surface-to-deep offset as more
18 light carbon is being pumped into the ocean interior although this is unlikely to be the sole cause of
19 the elevated gradients; more complete remineralisation should serve to reduce the $\delta^{13}\text{C}_{\text{DIC}}$ in the
20 deeper ocean rather than elevate surface values. Instead, the surface ocean $\delta^{13}\text{C}_{\text{DIC}}$ could have been
21 elevated due to higher rates of primary productivity which would have transferred proportionally
22 more ^{12}C to organic tissues than occurs today. This would imply higher oceanic nutrient availability,
23 perhaps from enhanced silicate weathering under greenhouse climates (e.g., [99, 100, 102, 103]) or
24 efficient turnover of deep waters [104]. Alternatively, oceanic DIC concentrations could have been
25 generally lower in the Eocene, as indicated by some carbon cycle models (e.g., [100]), which would
26 enhance observed $\delta^{13}\text{C}_{\text{DIC}}$:depth gradients even without a change in rates of primary productivity in
27 the surface ocean. This remains a possibility although several models suggest broadly unchanged
28 DIC (and alkalinity) over the Cenozoic [105].
29
30
31
32
33
34
35
36
37
38
39

40 In summary, our data from the warm Eocene ocean provide prima facie support for the idea that the
41 remineralisation of sinking organic carbon in the water column was much more efficient than is
42 currently the case. We plan to investigate this possibility further by incorporating metabolic rate
43 effects into carbon cycle models. Models should also be used to take into account other controls on
44 the shape of the $\delta^{13}\text{C}_{\text{DIC}}$: depth profile, many of which may relate to elevated water temperatures,
45 such as changes in oceanic circulation and enhanced oceanic stratification. This information about
46 warm climates from the past may have important implications for the future: if anthropogenic
47 emissions move the world oceans towards warm Eocene-like conditions, there may be similar
48 profound consequences for water column structure and biological activity, and potentially far-
49 reaching effects on the marine carbon cycle.
50
51
52
53
54
55
56
57

58 **Acknowledgements:**

59
60

1 We thank M. Huber and J. Tindall for their contribution to the Eocene modelled temperature:depth
2 profiles. This work was supported by a NERC standard grant awarded to GLF and PNP.
3
4
5
6
7
8
9
10
11
12
13
14
15
16
17
18
19
20
21
22
23
24
25
26
27
28
29
30
31
32
33
34
35
36
37
38
39
40
41
42
43
44
45
46
47
48
49
50
51
52
53
54
55
56
57
58
59
60

For Review Only

References:

1. Kleypas, J.A., Buddemeier, R.W., Archer, D., Gattuso, J.-P., Langdon, C., Opdyke, B.N., 1999. Geochemical Consequences of Increased Atmospheric Carbon Dioxide on Coral Reefs. *Science* **284**, 117-120.
2. Caldeira, K. and Wickett, M. E., 2003. Anthropogenic carbon and ocean pH. *Nature* **425**, 365.
3. Laws, E. A., Falkowski, P. G., Smith, W. O., Ducklow, H. and McCarthy, J. J., 2000. Temperature effect on export production in the open ocean. *Global Biogeochemical Cycles* **14**, 1231–1246.
4. Matsumoto, K., 2007. Biology-mediated temperature control on atmospheric $p\text{CO}_2$ and ocean biogeochemistry. *Geophysical Research Letters* **34**. L20605.
5. Young Kwon, E., Primeau, F. and Sarmiento, J.L., 2009. The impact of remineralisation depth on the air sea carbon balance. *Nature Geoscience* **2**, 630-635.
6. Regaudie-de-Gioux, A. and Duarte, C.M., 2012. Temperature dependence of planktonic metabolism in the ocean. *Global Biogeochemical Cycles* **26**, GB1015.
7. Sloan, L.C., and Rea, D.K., 1995. Atmospheric carbon dioxide and early Eocene climate: A general circulation modeling sensitivity study. *Palaeogeography, Palaeoclimatology, Palaeoecology* **119**, 275-295.
8. Markwick, P. J., 1998. Fossil crocodylians as indicators of Late Cretaceous and Cenozoic climates: implications for using palaeontological data in reconstructing palaeoclimate. *Palaeogeography, Palaeoclimatology, Palaeoecology* **137**, 205–271.
9. Huber, M., 2009. Climate change: Snakes tell a torrid tale. *Nature* **457**, 669-671.
10. Greenwood, D.R., 2007. Fossil angiosperm leaves and climate: From Wolfe and Dilcher to Burnham and Wilf. *Courier Forschungsinstitut Senckenberg* **258**, 95–10.
11. Shackleton, N.J. and Kennett, J.P., 1975. Paleotemperature history of the Cenozoic and the initiation of Antarctic glaciation: oxygen and carbon isotope analyses in DSDP sites 277, 279, and 281. *Initial Reports of the Deep Sea Drilling Project* **29**, 743-755.
12. Pearson, P., 2012. Oxygen isotopes in foraminifera: Overview and Historical Review. In: Ivany, L.C. and Huber, B.T. (eds.). *Reconstructing Earth's Deep-Time Climate – The State of the Art in 2012. Paleontological Society Papers* **18**, 1-38.
13. Zachos, J., Pagani, M., Sloan, L., Thomas, E. and Billups, K., 2001. Trends, rhythms, and aberrations in global climate 65 Ma to present. *Science* **292**, 686–693.
14. Zachos, J.C., Dickens, G.R. and Zeebe, R.E., 2008. An early Cenozoic perspective on greenhouse warming and carbon-cycle dynamics. *Nature* **451**, 279-283.

15. Bohaty, S. M., and Zachos, J.C., 2003. Significant Southern Ocean warming event in the late middle Eocene. *Geology* **31**, 1017–1020.
16. Edgar, K., Wilson, P., Sexton, P., Gibbs, S., Roberts, A., Norris, R., 2010. New biostratigraphic, magnetostratigraphic and isotopic insights into the Middle Eocene Climatic Optimum in low latitudes. *Palaeogeography, Palaeoclimatology, Palaeoecology* **297**, 670–682.
17. Pearson, P.N., van Dongen, B.E., Nicholas, C.J., Pancost, R.D., Schouten, S., Singano, J.M., and Wade, B.S., 2007. Stable warm tropical climate through the Eocene epoch. *Geology* **35**, 211–214.
18. Bijl, P.K., Schouten, S., Sluijs, A., Reichert, G.-J., Zachos, J.C., and Brinkhuis, H., 2009. Early Palaeogene temperature evolution of the southwest Pacific Ocean. *Nature* **461**, 776–779.
19. Liu, Z., Pagani, M., Zinniker, D., DeConto, R. M., Huber, M., Brinkhuis, H., Shah, S. R., Leckie, R. M., and Pearson, A., 2009. Global Cooling During the Eocene-Oligocene Climate Transition. *Science* **323**, 1187–1190.
20. Emanuel, K., Des Autels, C., Holloway, C. and Korty, R., 2004. Environmental Control of Tropical Cyclone Intensity. *Journal of Atmospheric Sciences* **61**, 843–858.
21. Sriviver, R.L., and Huber, M., 2007. Observational evidence for an ocean heat pump induced by tropical cyclones. *Nature* **447**, 557–580.
22. Sigman, D.M. and Haug, G.H. 2003. The Biological Pump in the Past. In: Holland, H.D. and Turekian, K.K. (eds); Elderfield, H. (Volume Editor). *Treatise On Geochemistry*. Elsevier Science, Oxford. p. 491–528.
23. Olivarez Lyle, A. and Lyle, M.W., 2006. Missing organic carbon in Eocene marine sediments: Is metabolism the biological feedback that maintains end-member climates? *Paleoceanography* **21**, PA2007.
24. Stanley, S.M., 2010. Relation of Phanerozoic stable isotope excursions to climate, bacterial metabolism, and major extinctions. *Proceedings of the National Academy of Sciences of the USA* **107**, 19185–19189.
25. Spero, H.J., Lerche, I., and Williams, D.F., 1991. Opening the carbon isotope “vital effect” black box, 2. Quantitative model for interpreting foraminiferal carbon isotope data. *Paleoceanography* **6**, 639–655.
26. Arrhenius, S., 1889. Uber die Reaktionsgeschwindigkeit bei der Inversion von Rohrzucker durch Säuren. *Zeitschrift für physikalische Chemie* **4**, 226–248.
27. Hargrave B.T., 1969. Similarity of oxygen uptake by benthic communities. *Limnology and Oceanography* **14**, 801–805.
28. Singh, J. S., and Gupta, S. R., 1977. Plant decomposition and soil respiration in terrestrial ecosystems. *Botanical Reviews* **43**, 449–528.

- 1
2
3
4
5
6
7
8
9
10
11
12
13
14
15
16
17
18
19
20
21
22
23
24
25
26
27
28
29
30
31
32
33
34
35
36
37
38
39
40
41
42
43
44
45
46
47
48
49
50
51
52
53
54
55
56
57
58
59
60
29. Swart, P.K., 1983. Carbon and oxygen isotope fractionation in scleractinian corals: a review. *Earth-Science Reviews* **19**, 51-80.
 30. Hobbie, J.E. and Cole, J.J., 1984. Response of a detrital food web to eutrophication. *Bulletin of Marine Science* **35**, 357-363.
 31. White, P.A., Kalff, J., Rasmussen, J.B. and Gasol, J.M. 1991. The effect of temperature and algal biomass on bacterial production and specific growth rate in freshwater and marine habitats. *Microbial Ecology* **21**, 99-118.
 32. Brown, J. H., Gillooly, J. F., Allen, A. P., Savage, V. M. and West, G. B., 2004. Toward a metabolic theory of ecology. *Ecology* **85**, 1771–1789.
 33. Gillooly, J. F., Brown, J. H., West, G. B., Savage, V. M. and Charnov, E. L., 2001. Effects of size and temperature on metabolic rate. *Science* **293**, 2248–2251.
 34. Gillooly, J. F., Charnov, E. L., West, G. B., Savage, V. M., and Brown, J. H., 2002. Effects of size and temperature on developmental time. *Nature* **417**, 70–73.
 35. Harris, L.A., Duarte., C.M., Nixon, S.W., 2006. Allometric laws and prediction in estuarine and coastal ecology. *Estuaries and Coasts* **29**, 340–344.
 36. López-Urrutia, A., San Martin, E., Harris, R. P. and Irigoyen, X., 2006. Scaling the metabolic balance of the oceans. *Proceedings of the National Academy of Sciences of the U.S.A.* **103**, 8739–8744.
 37. Hoppe, H. G., Gocke, K., Koppe, R. and Begler, C., 2002. Bacterial growth and primary production along a north-south transect of the Atlantic Ocean. *Nature* **416**, 168–171.
 38. Chikamoto, M. O., Abe-Ouchi, A., Oka, A., and Smith, S. L., 2012. Temperature induced marine export production during glacial period. *Geophysical Research Letters* **39**, L21601, doi:10.1029/2012GL053828.
 39. Gu, G., Dickens, G.R., Bhatnagar, G., Colwell, F.S., Hirasaki, G.J. and Chapman, W.G., 2011. Abundant Early Palaeogene marine gas hydrates despite warm deep-ocean temperatures. *Nature Geoscience* **4**, 848-851.
 40. Berner, R.A., and Caldeira, K., 1997. The need for mass balance and feedback in the geochemical carbon cycle. *Geology* **25**, 955-956.
 41. Armstrong, R. A., Lee, C. Hedges, J. L., Honjo, S. and Wakeham, S. G., 2002. A new, mechanistic model for organic carbon fluxes in the ocean, based on the quantitative association of POC with ballast minerals. *Deep Sea Research Part II* **49**, 219–236.
 42. François, R., Honjo, S., Krishfield, R. and Manganini, S., 2002. Factors controlling the flux of organic carbon to the bathypelagic zone of the ocean. *Global Biogeochemical Cycles* **16**, 1087.
 43. Klaas, C., and Archer, D., 2002. Association of sinking organic matter with various types of mineral ballast in the deep sea: Implications for the rain ratio. *Global Biogeochemical Cycles*

- 1
2
3
4
5
6
7
8
9
10
11
12
13
14
15
16
17
18
19
20
21
22
23
24
25
26
27
28
29
30
31
32
33
34
35
36
37
38
39
40
41
42
43
44
45
46
47
48
49
50
51
52
53
54
55
56
57
58
59
60
- 16, GA1116.
44. Wilson, J. D., Barker, S. and Ridgwell, A., 2012. Assessment of the spatial variability in particulate organic matter and mineral sinking fluxes in the ocean interior: Implications for the ballast hypothesis. *Global Biogeochemical Cycles* **26**, GB4011, doi:10.1029/2012GB004398.
45. Hemleben, Ch., Spindler, M., and Anderson, O.R., 1989. *Modern Planktonic Foraminifera*. Springer Verlag, Berlin, 363 pp.
46. Emiliani C., 1954. Depth habitats of some species of pelagic foraminifera as indicated by oxygen isotope ratios. *American Journal of Science* **252**, 149–158.
47. Zeebe, R.E., Bijma, J., and Wolf-Gladrow, D.A., 1999. A diffusion-reaction model of carbon isotope fractionation in foraminifera. *Marine Chemistry* **64**, 199–227.
48. Birch, H., Coxall, H., Pearson, P. and Kroon, D., *in press*. Planktonic foraminifera stable isotopes and water column structure: disentangling ecological signals. *Marine Micropaleontology*.
49. Wade, B.S. and Pearson, P.N., 2008. Planktonic foraminiferal turnover, diversity fluctuations and geochemical signals across the Eocene/Oligocene boundary in Tanzania. *Marine Micropaleontology* **68**, 244-255.
50. Pearson, P.N., Ditchfield, P., Singano, J., Harcourt-Brown, K., Nicholas, C., Olsson, R., Shackleton, N. J., and Hall, M., 2001. Warm tropical sea surface temperatures in the Late Cretaceous and Eocene epochs. *Nature* **413**, 481–487.
51. Bown, P.R., Dunkley Jones, T., Lees, J.A., Randell, R.D., Mizzi, J.A., Pearson, P.N., Coxall, H.K., Young, J.R., Nicholas, C.J., Karega, A., Singano, J. and Wade, B.S., 2008. A Paleogene calcareous microfossil Konservat-Lagerstätte from the Kilwa Group of coastal Tanzania. *Geological Society America Bulletin* **120**, 3–12.
52. Sexton, P.F., Wilson, P.A., Pearson, P.N., 2006. Palaeoecology of late middle Eocene planktic foraminifera and evolutionary implications. *Marine Micropaleontology* **60**, 1–16.
53. Hilting, A.K., Kump, L.R. and Bralower, T.J., 2008. Variations in the oceanic vertical carbon isotope gradient and their implications for the Paleocene-Eocene biological pump. *Paleoceanography* **23**, PA3222.
54. Pearson, P. N., Nicholas, C. J., Singano, J. M., Bown, P. R., Coxall, H. K., van Dongen, B. E., Huber, B.T., Karega, A., Lees, J. A., Msaky, E., Pancost, R.D., Pearson, M., and Roberts, A. P., 2004. Paleogene and Cretaceous sediment cores from the Kilwa and Lindi areas of coastal Tanzania: Tanzania Drilling Project Sites 1-5, *Journal of African Earth Sciences* **39**, 25-62.
55. Nicholas, C.J., Pearson, P.N., Bown, P.R., Jones, T.D., Huber, B.T., Karega, A., Lees, J.A., McMillan, I.K., O'Halloran, A., Singano, J.M. and Wade, B.S., 2006. Stratigraphy and

- 1 sedimentology of the Upper Cretaceous to Paleogene Kilwa Group, southern coastal Tanzania.
2
3
4 *Journal of African Earth Sciences* **45**, 431-466.
- 5 56. Wade, B.S., Pearson, P.N., Berggren, W.A., and Pälike, H., 2011. Review and revision of
6 Cenozoic tropical planktonic foraminiferal biostratigraphy and calibration to the Geomagnetic
7 Polarity and Astronomical Time Scale. *Earth Science Reviews* **104**, 111-142.
- 8
9
10 57. Erez, J., Luz, B., 1983. Experimental paleotemperature equation for planktonic foraminifera.
11 *Geochimica et Cosmochimica Acta* **47**, 1025-1031.
- 12
13 58. Berger, W.H., Killingley, J.S. and Vincent, E., 1978. Stable isotopes in deep-sea carbonates: box
14 core ERDC-92, West equatorial Pacific. *Oceanologica Acta* **1**, 203-216.
- 15
16
17 59. Wefer, G., Berger, W.H., 1991. Isotope paleontology: growth and composition of extant
18 calcareous species. *Marine Geology* **100**, 207-248.
- 19
20
21 60. Ortiz, J.D., Mix, A.C., Rugh, W., Watkins, J.M., and Collier, R.W., 1996. Deep-dwelling
22 planktonic foraminifera of the northeastern Pacific Ocean reveal environmental control of
23 oxygen and carbon isotopic disequilibria. *Geochimica et Cosmochimica Acta* **60**, 4509-4523.
- 24
25
26 61. Spero, H.J., Bijma, J., Lea, D.W., and Bemis, B.E., 1997. Effect of seawater carbonate
27 concentration on foraminiferal carbon and oxygen isotopes. *Nature* **390**, 497-500.
- 28
29
30 62. Schmidt, D.N.F., Elliott, T.R. and Kasemann, S.A., 2008. The influences of growth on planktic
31 foraminifers as proxies for palaeostudies. In: James, R. H., Austin, W.E.N., Clarke, Leon J.,
32 Rickaby, R. E. M. (eds.), *Biogeochemical Controls on Palaeoceanographic Proxies* **303**, 73-85,
33 Geological Society of London.
- 34
35
36 63. Pearson, P.N., and Wade, B.S., 2009. Taxonomy and stable isotope paleoecology of well-
37 preserved planktonic foraminifera from the uppermost Oligocene of Trinidad. *Journal of*
38 *Foraminiferal Research* **39**, 191-217.
- 39
40
41 64. Bé, A.W.H., 1982. Biology of planktonic foraminifera. In: Buzas, M.A., Sen Gupta, B.K.,
42 Broadhead, T.W. (eds.). *Foraminifera notes for a short course*. University of Tennessee,
43 Knoxville, pp. 51-89.
- 44
45
46 65. Bouvier-Soumagnac, Y., and Duplessy, J.C., 1985. Carbon and oxygen isotopic composition of
47 planktonic foraminifera from laboratory culture, plankton tows and recent sediment:
48 implications for the reconstruction of paleoclimatic conditions and of the global carbon cycle.
49 *Journal of Foraminiferal Research* **15**, 302-320.
- 50
51
52 66. Spero, H.J., and Williams, D.F., 1988. Extracting environmental information from planktonic
53 foraminiferal $\delta^{13}\text{C}$ data. *Nature* **335**, 717-719.
- 54
55
56 67. D'Hondt, S., Zachos, J.C. and Schultz, G., 1994. Stable isotopic signals and photosymbiosis in
57 Late Paleocene planktic foraminifera. *Palaeobiology* **20**, 391-406.
- 58
59
60 68. Norris, R. D., 1996. Symbiosis as an evolutionary innovation in the radiation of Paleocene

- 1 planktic Foraminifera. *Paleobiology* **22**, 461–48.
- 2
- 3 69. Spero, H.J. and Lea, D.W., 1996. Experimental determination of stable isotope variability in
- 4 *Globigerina bulloides*: Implications for paleoceanographic reconstructions. *Marine*
- 5 *Micropaleontology* **28**, 231-246.
- 6
- 7
- 8 70. Bijma, J., Spero, H.J., Lea, D.W., 1999. Reassessing foraminiferal stable isotope geochemistry:
- 9 impact of the oceanic carbonate system (experimental results). In: Fischer, G., Wefer, G. (eds.).
- 10 *Use of Proxies in Paleoceanography: Examples from the South Atlantic*. Springer, New York,
- 11 489–521.
- 12
- 13
- 14 71. Duplessy, J. C., Delibrias, G., Turon, J. L., Pujol, C. and Duprat, J. 1981. Deglacial warming of
- 15 the northeastern Atlantic ocean: correlation with the paleoclimatic evolution of the european
- 16 continent. *Palaeogeography, Palaeoclimatology, Palaeoecology* **35**, 121–144.
- 17
- 18 72. Kroon, D. and Darling, K., 1995. Size and environmental control of the stable isotope signal
- 19 related to test size in *Neogloboquadrina dutertrei* (d'Orbigny) and *Globigerinoides ruber*
- 20 d'Orbigny. *Journal of Foraminiferal Research* **25**, 39-52.
- 21
- 22
- 23 73. Triantaphyllou, M.V., Antonarakou, A., Dimiza, M. and Anagnostou Ch., 2010. Calcareous
- 24 nannofossil and planktonic foraminiferal distributional patterns during deposition of sapropels
- 25 S6, S5 and S1 in the Libyan Sea (Eastern Mediterranean). *Geo-Marine Letters* **30**, 1-13.
- 26
- 27 74. Chaisson, W.P., Ravelo, A.C., 1997. Changes in upper water-column structure at Site 925, late
- 28 Miocene–Pleistocene: Planktonic foraminifer assemblage and isotopic evidence. In: Shackleton,
- 29 N.J., Curry, W.B., Richter, C., Bradower, T.J. (eds.). *Proceedings of ODP Scientific Results*
- 30 **154**, 255–268.
- 31
- 32 75. Pearson P. and Wade, B., 2009. Taxonomy and stable isotope paleoecology of well-preserved
- 33 planktonic foraminifera from the uppermost oligocene of Trinidad. *The Journal of*
- 34 *Foraminiferal Research* **39**, 191-217.
- 35
- 36
- 37 76. Birch, H.B., Coxall, H.K. and Pearson, P.N., 2012. Evolutionary ecology of Early Paleocene
- 38 planktonic foraminifera: Size, depth habitat and symbiosis. *Paleobiology* **38**, 374-390.
- 39
- 40 77. Kim, S.-T. and O'Neil, J.R., 1997. Equilibrium and non-equilibrium oxygen isotope effects in
- 41 synthetic carbonates. *Geochimica et Cosmochimica Acta* **61**, 3461-3475.
- 42
- 43 78. Cramer, B.S., Miller, K.G., Barrett, P.J., and Wright, J.D., 2011. Late Cretaceous–Neogene
- 44 trends in deep ocean temperature and continental ice volume: reconciling records of benthic
- 45 foraminiferal geochemistry ($\delta^{18}\text{O}$ and Mg/Ca) with sea level history. *Journal of Geophysical*
- 46 *Research-Oceans* **116**, C12023.
- 47
- 48 79. Zachos, J.C., Stott, L.D., Lohmann, K.C., 1994. Evolution of early Cenozoic marine
- 49 temperatures. *Paleoceanography* **9**, 353-387.
- 50
- 51
- 52
- 53
- 54
- 55
- 56
- 57
- 58
- 59
- 60

- 1
2
3
4
5
6
7
8
9
10
11
12
13
14
15
16
17
18
19
20
21
22
23
24
25
26
27
28
29
30
31
32
33
34
35
36
37
38
39
40
41
42
43
44
45
46
47
48
49
50
51
52
53
54
55
56
57
58
59
60
80. Tindall, J.C., Flecker, R., Valdes, P., Schmidt, D.N., Markwick, P. and Harris, J., 2010. Modelling the oxygen isotope distribution of ancient seawater using a coupled ocean–atmosphere GCM: Implications for reconstructing early Eocene climate. *Earth and Planetary Science Letters* **292**, 265–273.
81. Huber, M. and Caballero, R., 2011. The early Eocene equable climate problem revisited. *Climates of the Past Discussions* **7**, 241-304.
82. National Oceanographic Data Center. World Ocean Database 2009. http://www.nodc.noaa.gov/OC5/WOD09/pr_wod09.html
83. National Oceanographic Data Center. World Ocean Atlas 2009. http://www.nodc.noaa.gov/OC5/WOA09/pr_woa09.html
84. Pearson, P.N., Shackleton, N.J., and Hall, M.A., 1993. Stable isotope paleoecology of middle Eocene planktonic foraminifera and integrated isotope stratigraphy, DSDP Site 523, South Atlantic. *Journal of Foraminiferal Research* **23**, 123-140.
85. Wade, B.S., Al-Sabouni, N., Hemleben, C., and Kroon, D., 2008. Symbiont bleaching in fossil planktonic foraminifera. *Evolutionary Ecology* **22**, 253-265.
86. Olsson, R.K. and Hemleben, Ch., 2006. Taxonomy, biostratigraphy, and phylogeny of Eocene *Globanomalina*, *Planoglobanomalina*, n.gen. In: Pearson, P.N., Olsson, R.K., Huber, B.T., Hemleben, C., and Berggren, W.A. (eds.). Atlas of Eocene Planktonic Foraminifera. *Cushman Foundation Special Publication No. 41*, 413-432.
87. Huber, B.T., Olsson, R.K. and Pearson, P.N., 2006. Taxonomy, biostratigraphy, and phylogeny of Eocene microperforate planktonic foraminifera (*Jenkinsina*, *Cassigerinelloita*, *Chiloguembelina*, *Streptochilus*, *Zeauvigerina*, *Tenuitella*, and *Cassigerinella*) and problematic (*Dipsidripella*). In: Pearson, P.N., Olsson, R.K., Huber, B.T., Hemleben, C., and Berggren, W.A. (eds.) Atlas of Eocene Planktonic Foraminifera. *Cushman Foundation Special Publication No. 41*, 461-508.
88. Premoli Silva I., Wade B.S., Pearson P.N., 2006. Chapter 7: Taxonomy of *Globigerinatheka* and *Orbulinoides*. In: Pearson, P.N., Olsson, R.K., Huber, B.T., Hemleben, C., and Berggren, W.A. (eds.) Atlas of Eocene Planktonic Foraminifera. *Cushman Foundation Special Publication No. 41*, 461-508.
89. Wade, B.S. 2004. Planktonic foraminiferal biostratigraphy and mechanisms in the extinction of *Morozovella* in the late middle Eocene. *Marine Micropaleontology* **51**, 23-38.
90. Kroopnick, P.M., 1985. The distribution of $\delta^{13}\text{C}$ of ΣCO_2 in the world oceans. *Deep-Sea Research* **32**, 57-84.

- 1
2
3
4
5
6
7
8
9
10
11
12
13
14
15
16
17
18
19
20
21
22
23
24
25
26
27
28
29
30
31
32
33
34
35
36
37
38
39
40
41
42
43
44
45
46
47
48
49
50
51
52
53
54
55
56
57
58
59
60
91. Roberts, C., and Tripathi, A., 2009. Modelled reconstructions of the oceanic carbonate system for different histories of atmospheric carbon dioxide during the last 20 Ma. *Global Biogeochemical Cycles* **23**, GB1011.
 92. Sexton, P.F., Norris, R.D., Wilson, P.A., Pälike, H., Westerhold, T., Röhl, U., Bolton, C.T., and Gibbs, S., 2011. Eocene global warming events driven by ventilation of oceanic dissolved organic carbon. *Nature* **471**, 349-352.
 93. Kent, P.E., Hunt, J.A., and Johnstone, D.W., 1971. The Geology and Geophysics of Coastal Tanzania. *Institute of Geological Sciences Geophysical Paper No. 6*, i-iv, 1-101.
 94. Kroon, D. and the Shipboard Scientific Party, 2010. GLOW: Tropical Temperature History during Paleogene Global Warming (GLOW) Events. Site Survey Cruise Report, 151 pp.
 95. Derry, L. A. and France-Lanord, C., 1996. Neogene growth of the sedimentary organic carbon reservoir. *Paleoceanography* **11**, 267–275, doi:10.1029/95PA03839.
 96. Hayes, J.M., Strauss, H. and Kaufman, A.J., 1999. The abundance of ¹³C in marine organic matter and isotopic fractionation in the global biogeochemical cycle of carbon during the past 800 Ma. *Chemical Geology* **161**, 103–125.
 97. Quillévéré, F., Norris, R.D., Moussa, I., and Berggren, W.A., 2001. Role of photosymbiosis and biogeography in the diversification of early Paleogene acarininids (planktonic foraminifera). *Paleobiology* **27**, 311-326.
 98. Bornemann, A., Norris, R.D., 2007. Size-related stable isotope changes in Late Cretaceous planktic foraminifera: Implications for paleoecology and photosymbiosis. *Marine Micropaleontology* **65**, 32-42.
 99. François, L.M. and Goddérès, Y., 1998. Isotopic constraints on the Cenozoic evolution of the carbon cycle. *Chemical Geology* **145**, 177–212.
 100. Wallmann, K., 2001. Controls on the Cretaceous and Cenozoic evolution of seawater composition, atmospheric CO₂ and climate. *Geochimica et Cosmochimica Acta* **65**, 3005-3025.
 101. Raymo, M.E. and Ruddiman, W.F., 1992. Tectonic Forcing of late Cenozoic climate. *Nature* **359**, 117-122.
 102. Misra, S. and Froelich, P.N., 2012. Lithium Isotope History of Cenozoic Seawater: Changes in Silicate Weathering and Reverse Weathering. *Science* **335**, 818-823.
 103. Föllmi, K.B., 1995. 160 m.y. record of marine sedimentary phosphorus burial: Coupling of climate and continental weathering under greenhouse and icehouse conditions. *Geology* **23**, 503-506.
 104. Huber, M., and Sloan, L. C., 2001. Heat transport, deep waters, and thermal gradients: Coupled simulation of an Eocene greenhouse climate. *Geophysical Research Letters* **28**, 3481–3484.

- 1
2
3
4
5
6
7
8
9
10
11
12
13
14
15
16
17
18
19
20
21
22
23
24
25
26
27
28
29
30
31
32
33
34
35
36
37
38
39
40
41
42
43
44
45
46
47
48
49
50
51
52
53
54
55
56
57
58
59
60
105. Tyrrell, T. and Zeebe, R.E., 2004. History of carbonate ion concentration over the last 100 million years. *Geochimica et Cosmochimica Acta* **68**, 3521-3530.
106. Pearson, P.N., Premec-Fucek, V. and Premoli Silva, S., 2006. Chapter 15: Taxonomy, biostratigraphy, and phylogeny of Eocene *Turborotalia*. In: Pearson, P.N., Olsson, R.K., Huber, B.T., Hemleben, C., and Berggren, W.A. (eds.) *Atlas of Eocene Planktonic Foraminifera. Cushman Foundation Special Publication No. 41*, 433-460.
107. Swart, P.K., Greer, L., Rosenheim, B.E., Moses, C.S. Moses, Waite, A.J., Winter, A., Dodge, R.E. and Helmle, K., 2010. The ^{13}C Suess effect in scleractinian corals mirror changes in the anthropogenic CO_2 inventory of the surface oceans. *Geophysical Research Letters* **37**, L05604.

For Review Only

Figure captions

Fig. 1. Schematic cartoon of the modern biological pump showing production of organic matter, its consumption by higher organisms and the respiration of CO₂. The profile on the right shows a $\delta^{13}\text{C}_{\text{DIC}}$ profile from a site offshore modern Tanzania (data taken from site 425 of [90]) to illustrate the typical decrease in $\delta^{13}\text{C}_{\text{DIC}}$ with depth due to preferential fixation of isotopically light carbon in the surface ocean during photosynthesis and the subsequent return of this light carbon as sinking organic matter is respired by microbes.

Fig. 2. Multi-species $\delta^{18}\text{O}$ and $\delta^{13}\text{C}$ crossplot for a modern core-top foraminifera assemblage from ~200 km offshore Tanzania (Latitude 8°51.5538'S Longitude 41°26.4102'E) at a water depth of 3006 m [94] Modified from Figure 7 of Birch et al. ([48]; full caption given therein). The site is oligotrophic, as shown by the CTD (conductivity temperature depth probe) data and the assemblage composition, which is dominated by typical oligotrophic species with only a very minor fraction of species that represent seasonal upwelling (e.g., *Globigerinita glutinata*). Planktonic foraminifera $\delta^{18}\text{O}$ values were converted to temperature according to the relationship of Erez and Luz [57] and using a modern seawater $\delta^{18}\text{O}_w$ value of 0.47 ‰. The grey band represents a composite water column $\delta^{13}\text{C}_{\text{DIC}}$ measurements taken from 7 sites within ~ 800 km of their study site (from World Ocean Database) and incorporating a +/- 0.5‰ window to account for seasonal variations. Data points falling outside of this band are thought to represent calcification out of isotopic equilibrium with DIC or by foraminifera that calcified during episodes of seasonal upwelling (i.e., *G. bulloides* and *G. glutinata*). For the species with obligate symbionts (*), the largest individuals have $\delta^{13}\text{C}$ values up to 1.0 ‰ higher than the equilibrium envelope due to photosynthetic activity by symbiotic algae. The smallest individuals of most species have $\delta^{13}\text{C}$ values that are 0.2-2.0 ‰ lower than the envelope because of size-related metabolic effects. The $\delta^{13}\text{C}$ measured in mid-sized shells (in the ~212-355 μm size fraction) in fossil assemblages should therefore provide the closest approximation of $\delta^{13}\text{C}_{\text{DIC}}$. *Gs.* = *Globigerinoides*, *Ga.* = *Globigerinita*, *Gt.* = *Globoturborotalita*, *O.* = *Orbulina*, *Gg.* = *Globigerina*, *Gr.* = *Globorotalia*; *Ge.* = *Globigerinella*, *Gd.* = *Globorotaloides*, *T.* = *Truncorotalia*.

Fig. 3. Cartoon showing how data points plotting in different fields of the $\delta^{18}\text{O}$ and $\delta^{13}\text{C}$ crossplots can be interpreted after Pearson and Wade [75].

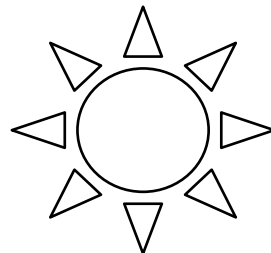
Fig. 4. A. Temperature:depth profiles from modern measurements from offshore Tanzania (CTD data from, 41° 77 E, 10° 65 S, water depth of 2219 m [94]) and those generated by the HadCM3

(dashed) and NCAR (solid) models [80, 81]. Only the NCAR profile produced using a 2240 ppmv $p\text{CO}_2$ climate forcing is illustrated here; the sea surface temperatures in the modelled profile are consistent with the temperatures derived from middle Eocene mixed layer foraminiferal $\delta^{18}\text{O}$ values. The profiles generated by 1120 ppmv (used for the late Eocene timeslice) and 4480 ppmv (used for the early Eocene timeslices) $p\text{CO}_2$ simply shift the profile to higher or lower temperatures. B. Temperature:depth profile for the modern (a composite of 7 measured depth profiles from the World Ocean Database 2009 [82] between 19.5 and 22.5 N and -95.5 and -96.5 W) and profile generated by the NCAR model for the middle Eocene [81].

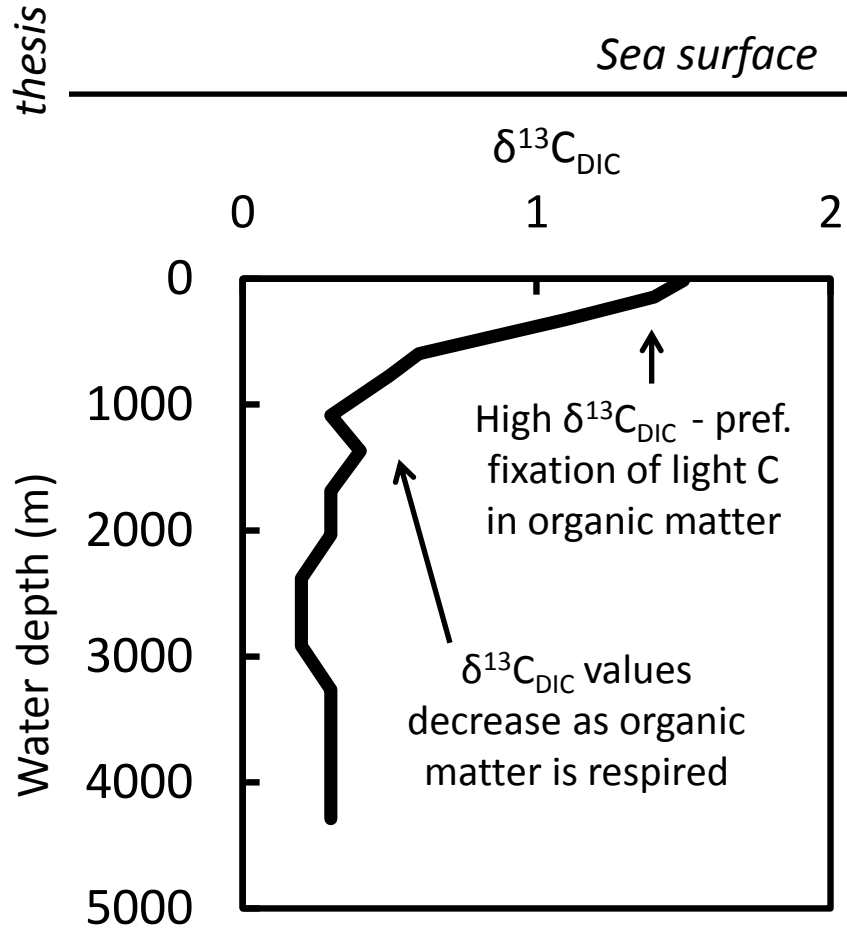
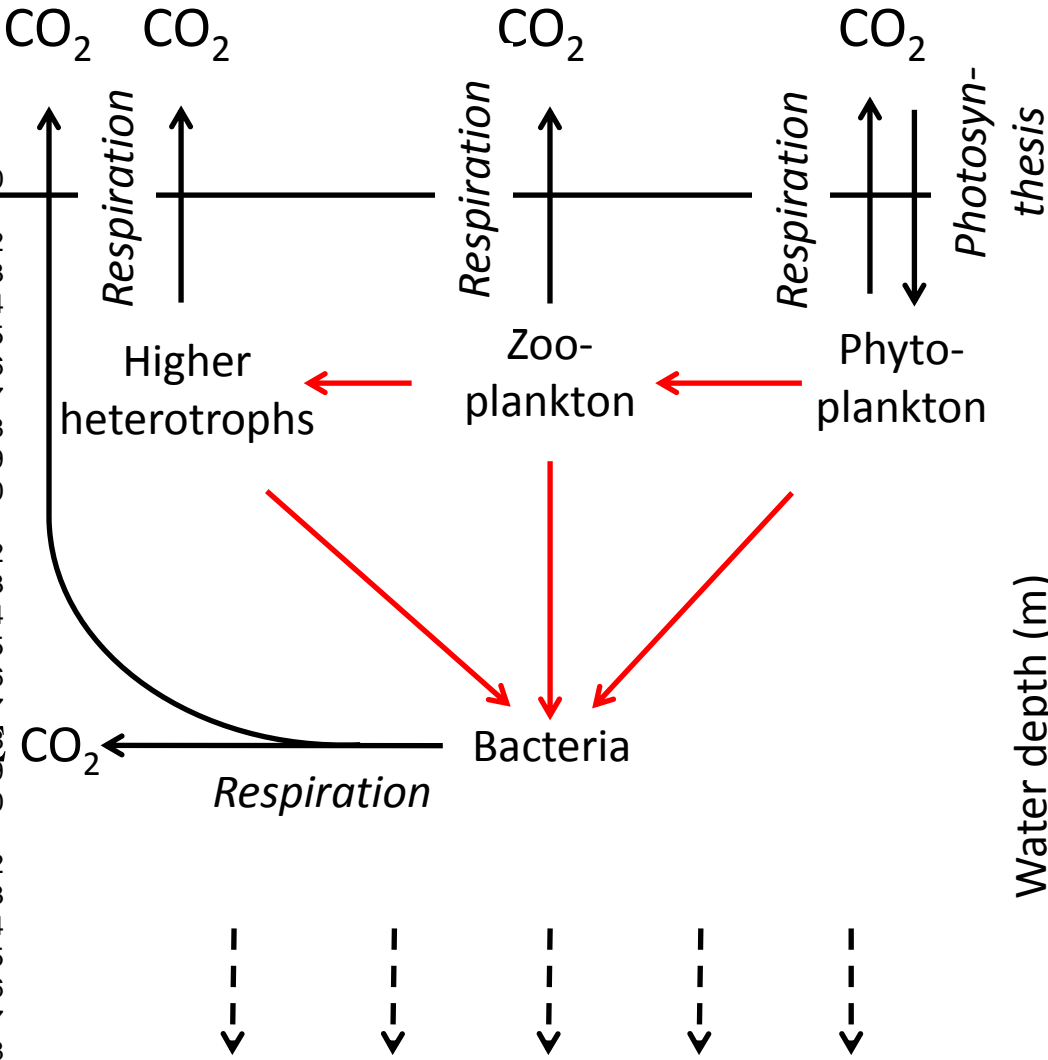
Fig. 5. A-H. Step-by-step reconstruction of $\delta^{13}\text{C}$:depth gradients using this data and modelled temperature:depth profiles. i) Cross plots of $\delta^{13}\text{C}$ and $\delta^{18}\text{O}$ data from Pearson et al. [50], Pearson et al. [17] and Wade and Pearson [49] showing names of multiple species of planktonic (and benthic) foraminifera and the size fraction in which they were analysed (given in μm), where appropriate. Note that in Fig. 5H, species names have been updated from the original dataset in Pearson et al., [50]. **Ps. pseudowilsoni* in this case was originally named *Paragloborotalia pseudomayeri* in Pearson et al. [50]. Strictly speaking, *Pa. pseudomayeri* is a synonym of *Turborotalia pomeroli* [106] but at the time of data collection, the authors [50] actually designated this species name to what would now be referred to as *Ps. pseudowilsoni*. A. = *Acarinina*; C = *Catapsydrax*; Cb = *Cribohantkenina*; Cg = *Chiloguembelina*; Ga. = *Globoturborotalita*; Gk. = *Globigerinatheka*; Gm. = *Guembelitrioides*; I. = *Igorina*; M. = *Morozovellain* A-C, *Morozovelloides* in D-F; Pg. = *Planoglobanomalina*; Ph. = *Pseudohastigerina*; Ps. = *Parasubbotina*; S. = *Subbotina*; Ta. = *Turborotalita*. ii) The same cross plots redrawn to show mixed layer temperature (generated from the lowest $\delta^{18}\text{O}$ value), denoted by a dashed line. Empty squares represent those data points that were not used to construct the final $\delta^{13}\text{C}$ profile following the criteria of Birch et al. (2012). Note that no data points were eliminated from the Guayabal Formation assemblage (H) because during the initial data collection, foraminifera were chosen from all size fractions $>250 \mu\text{m}$. iii) Temperature:depth profile showing how the $\delta^{18}\text{O}$ -generated temperatures were used to generate absolute depths. iv) $\delta^{13}\text{C}$:depth profiles for each sample (black) and the modern profile (green) for offshore Tanzania (averaged profile from several nearby sites). Note that studies suggest that surface Indian Ocean $\delta^{13}\text{C}_{\text{DIC}}$ values have decreased by $\sim 0.6 \text{‰}$ since 1900 [107] due to the ‘Suess effect’ i.e. the influence of isotopically light carbon emitted through burning fossil fuels. This has not been included in the figure but should be noted.

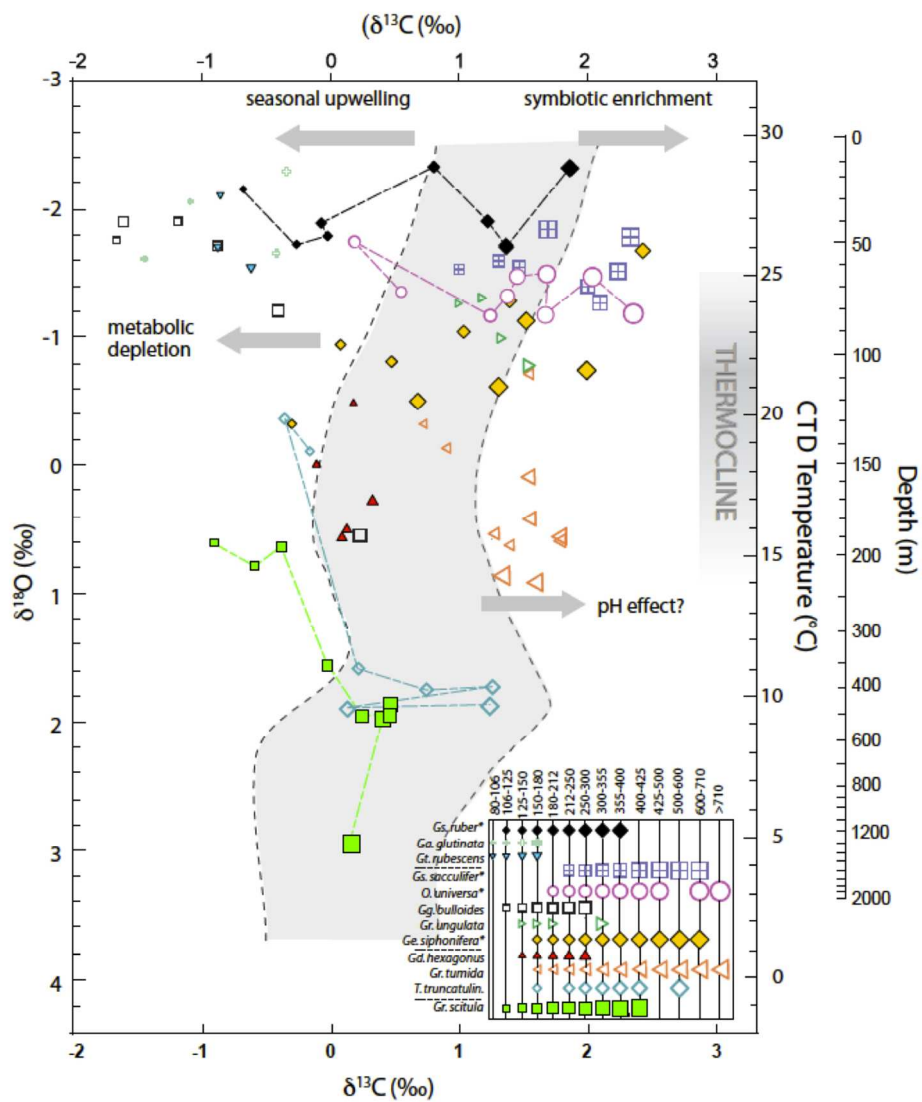
1
2
3
4
5
6
7
8
9
10
11
12
13
14
15
16
17
18
19
20
21
22
23
24
25
26
27
28
29
30
31
32
33
34
35
36
37
38
39
40
41
42
43
44
45
46
47
48
49
50
51
52
53
54
55
56
57
58
59
60

For Review Only



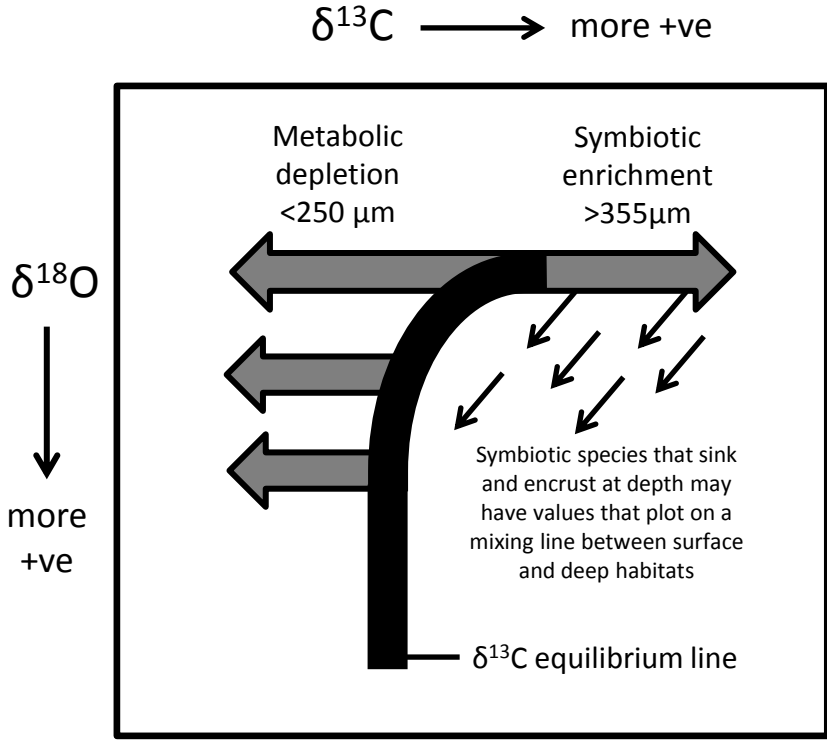
1
2
3
4
5
6
7
8
9
10
11
12
13
14
15
16
17
18
19
20
21
22
23
24
25
26
27
28
29
30
31
32
33
34
35
36
37
38
39
40
41
42
43





242x305mm (150 x 150 DPI)

1
2
3
4
5
6
7
8
9
10
11
12
13
14
15
16
17
18
19
20
21
22
23
24
25
26
27
28
29
30
31
32
33
34
35
36
37
38
39
40
41
42
43

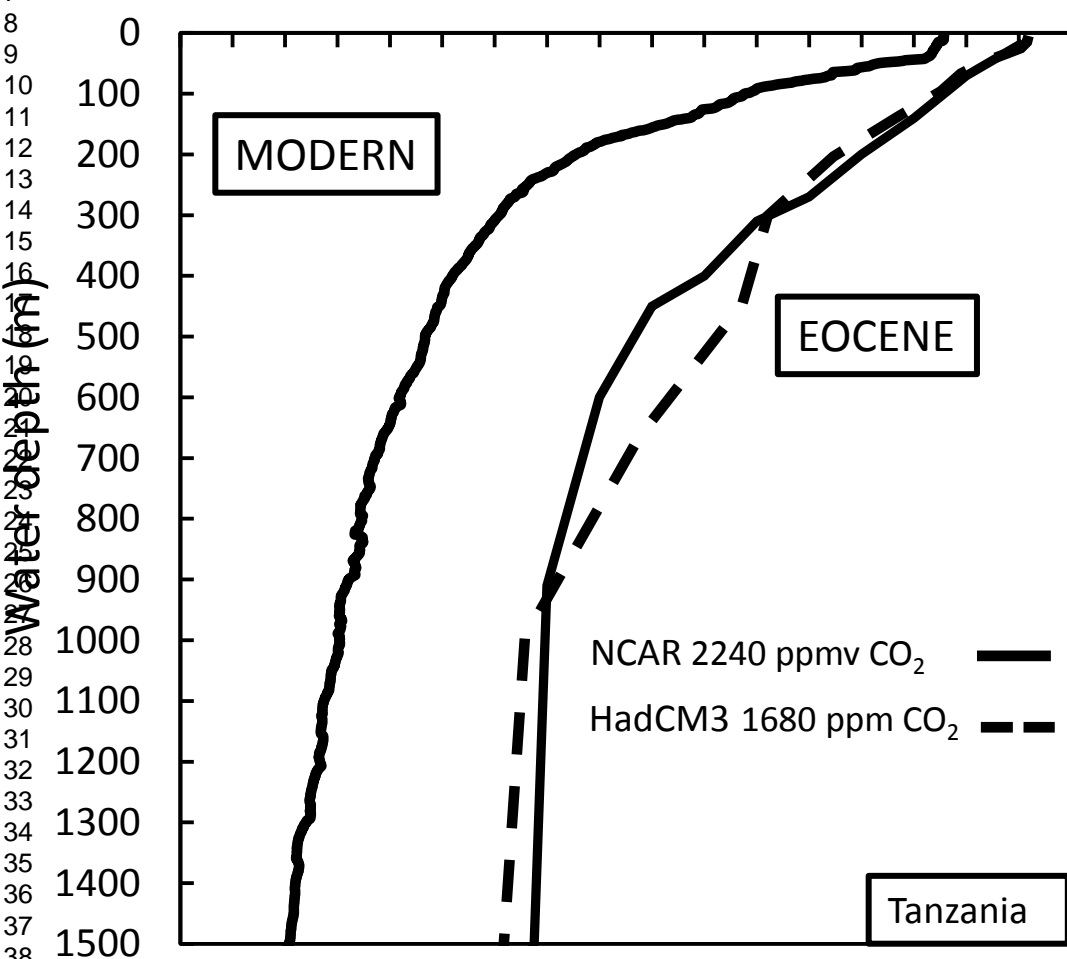


1
2
3
4
5
6
7
8
9
10
11
12
13
14
15
16
17
18
19
20
21
22
23
24
25
26
27
28
29
30
31
32
33
34
35
36
37
38
39
40
41
42
43

Water T (°C)

0 2 4 6 8 10 12 14 16 18 20 22 24 26 28 30 32 34

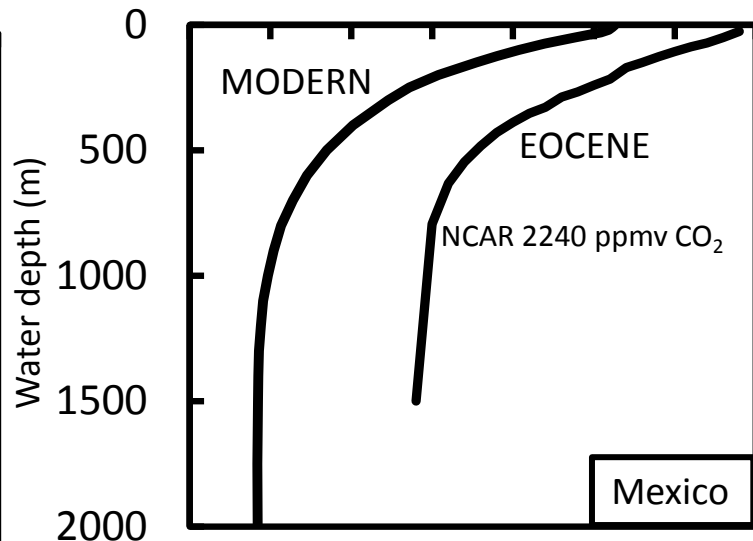
A



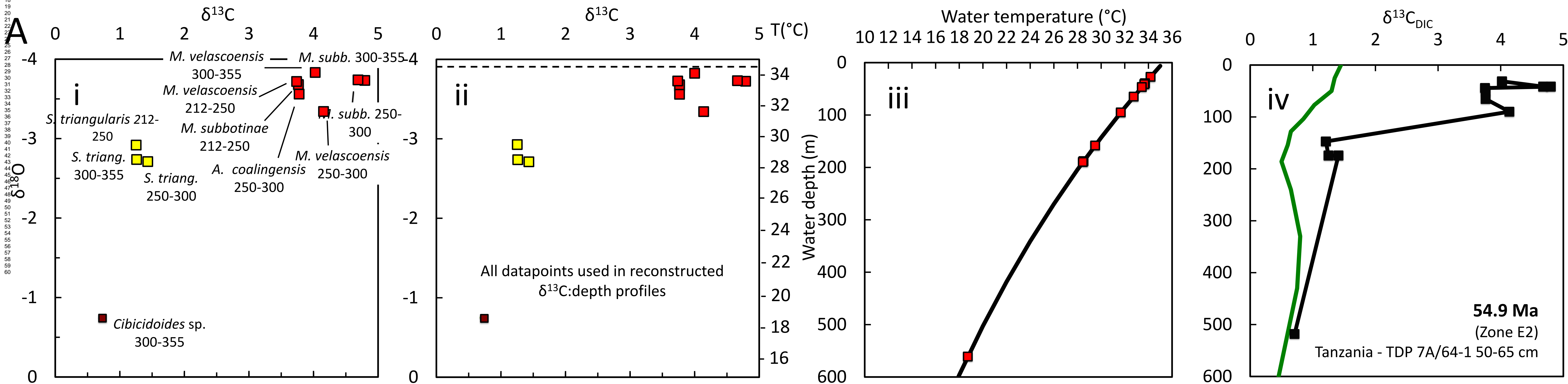
Water T (°C)

0 5 10 15 20 25 30 35

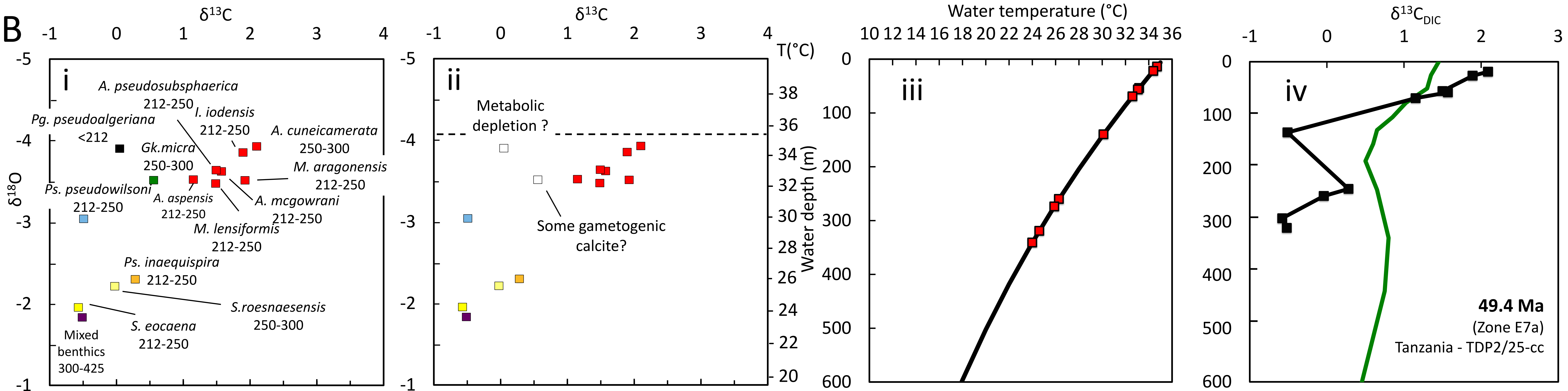
B



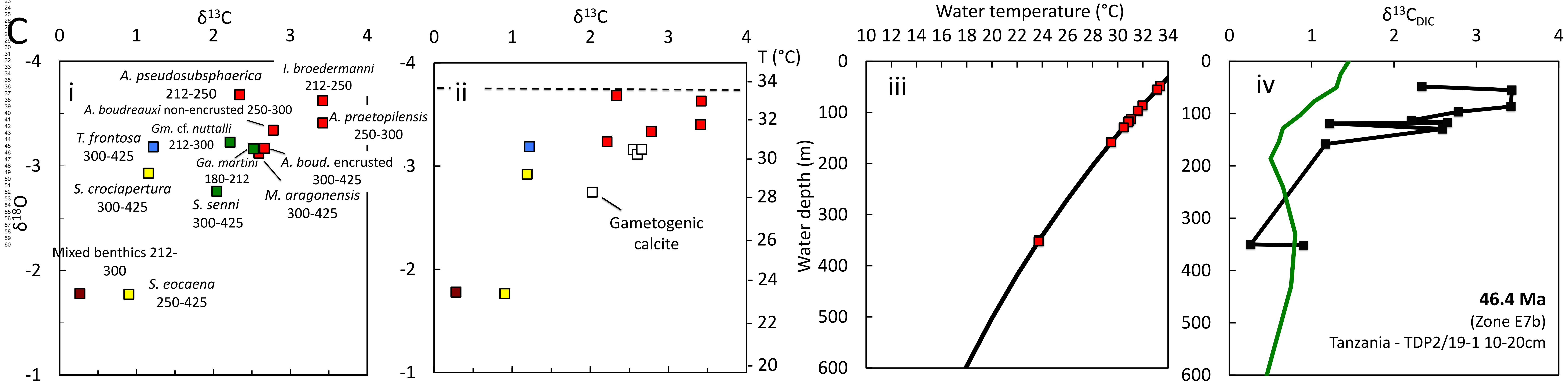
A



B



C



D

